The Structure of a Mutant Photosynthetic Reaction Center Shows Unexpected Changes in Main Chain Orientations and Quinone Position†

P. R. Pokkuluri, P. D. Laible, Y.-L. Deng,‡ T. N. Wong, D. K. Hanson, and M. Schiffer*

Biosciences Division, Argonne National Laboratory, 9700 South Cass Avenue, Argonne, Illinois 60439

Received October 8, 2001; Revised Manuscript Received February 18, 2002

ABSTRACT: We report on the unexpected structural changes caused by substitution of acidic amino acids in the Q_B binding pocket of the bacterial photosynthetic reaction center by alanines. The mutations targeted key residues L212Glu and L213Asp of this transmembrane protein−cofactor complex. The amino acid substitutions in the L212Ala-L213Ala mutant reaction center ("AA") were known to affect the delivery of protons after the light-induced generation of Q_B^-, which renders the AA strain incapable of photosynthetic growth. The AA structure not only revealed side chain rearrangements but also showed movement of the main chain segments that are contiguous with the mutation sites. The alanine substitutions caused an expansion of the cavity rather than its collapse. In addition, Q_B is found mainly in the binding site that is proximal to the iron−ligand complex (closest to Q_A) as opposed to its distal binding site (furthest from Q_A) in the structure of the wild-type reaction center. The observed rearrangements in the structure of the AA reaction center establish a new balance between charged residues of an interactive network near Q_B. This structurally and electrostatically altered complex forms the basis for future understanding of the structural basis for proton transfer in active reaction centers which retain the alanine substitutions but carry a distant compensatory mutation.

The bacterial photosynthetic reaction center from purple non-sulfur bacteria has long served as a model for understanding protein-mediated electron and proton transfer. The three-dimensional structure of the transmembrane protein−cofactor reaction center (RC)[1] complex was determined previously (*1*−*7*). The RC complexes from *Rhodobacter* (*R.*)-*sphaeroides* and *R. capsulatus* consist of three protein subunits—L, M, and H. The L and M subunits are encoded by the *puf*L and *puf*M genes of the *puf* operon. These helical transmembrane subunits are related by an axis of approximate 2-fold symmetry. These 2 subunits sequester and influence the functions of 10 cofactors: 2 bacteriochlorophylls which form a special pair (P), 2 monomeric bacteriochlorophylls (B_A and B_B), 2 bacteriopheophytins (H_A and H_B), 2 quinones (Q_A and Q_B), a carotenoid molecule, and a non-heme iron atom. The cofactors are arranged in two symmetry-related branches, and only the A-branch cofactors are active in the primary steps of charge separation. When P is excited by absorption of a photon, an electron is transferred from P* to B_A and then to H_A within 3 ps. The electron then proceeds to Q_A and on to Q_B on slower time scales. The iron−ligand complex, which is located on the pseudo-2-fold axis, connects the Q_A and Q_B binding sites.

Although they are identical ubiquinone$_{10}$ molecules, Q_A and Q_B have different in situ properties that can be attributed to the protein environment that surrounds them. Q_A is a one-electron gate and is never protonated; Q_B accepts two electrons from successive turnovers of the RC, after which two protons are delivered to it via transport through the cytoplasmic region of the complex. This region is formed by the interface of the L, M, and H chains and is characterized by an abundance of polar and ionizable residues as well as several solvent channels (*4*, *6*, *8*). Specific residues—such as L212Glu, L213Asp, L223Ser, and H173Glu—that are important for proton transfer to the reduced quinone have been identified in RCs of *R. sphaeroides* (*9*−*14*) and *R. capsulatus* (*15*−*20*). RCs of these two species share functional homology and ∼90% sequence similarity in this region of the complex (*18*). In the native RC, proton delivery pathways that include water molecules have been suggested by the results of both spectroscopic [e.g., (*21*−*24*)] and structure determination (*4*, *6*, *25*) experiments.

Previously, we have investigated the mechanisms of electron and proton transfer to the quinones in native RCs by characterizing *R. capsulatus* RCs in which the key residues L212Glu and L213Asp were mutated (*17*−*20*). These acidic residues, located within 5−6 Å of Q_B, were shown to be important in delivery of the second and first protons, respectively, to the Q_B anions (*9*, *12*). In addition, they differentiate the environment of the binding pocket of Q_B from that of Q_A where the symmetry-related residues in the M chain are nonpolar alanines. The L212Glu-L213Asp→Ala-Ala mutations ("AA" strain) interrupt the native pathway

† Supported by the United States Department of Energy, Office of Biological and Environmental Sciences, under Contract W-31-109-ENG-38.

* To whom correspondence should be addressed. Phone: (630)-252-3883; Fax: (630)-252-5517; E-mail: mschiffer@anl.gov.

‡ Present address: Agouron Pharmaceuticals, Inc., La Jolla, CA.

[1] Abbreviations: *R.*, *Rhodobacter*; Ap, ampicillin; Cm, chloramphenicol; Km, kanamycin; Sp, spectinomycin; Tc, tetracycline; IMAC, immobilized metal affinity chromatography; LDAO, lauryldimethylamine *N*-oxide; Q_A, primary quinone acceptor; Q_B, secondary quinone acceptor; RC, reaction center; AA, L212Glu-L213Asp→Ala-Ala double mutant.

10.1021/bi0118963 CCC: $22.00
Published on Web 04/17/2002

Table 1: Plasmids and Strains Used in This Study

plasmid or strain	description	source
plasmids		
pJW1	13 kb of *R. sphaeroides* DNA carrying *puf* operon, pBR322 derivative, Ap^R	(*27*)
pRIRV	~5 kb *Eco*RI−*Eco*RV fragment of pJW1, pIBI25 derivative, Ap^R	this study
pHP45Ω	2.0 kb Ω element encoding spectinomycin resistance, pBR322 derivative, Ap^RSp^R	(*28*)
pSUP202	mobilizable cloning vector, pBR325 derivative, $Ap^RCm^RTc^R$	(*29*)
pS202	pSUP202 carrying interrupted *puf* operon, $Ap^RTc^RSp^R$	this study
pRK404	broad-host-range mobilizable vector, Tc^R	(*30*)
pRK404(E)	pRK404 derivative with distal *Eco*RI site filled, Tc^R	this study
pRK404(EH)	pRK404(E) derivative with *Hin*dIII site in polylinker filled, Tc^R	this study
pRKSCH/pHisRC	*puf* operon carrying polyhistidine-tagged RC-M gene, pRK404 derivative, Tc^R	(*9*, *31*, *32*)
pRKMluBgl	~5.7 kb *Eco*RI−*Hin*dIII fragment with wild-type *puf* operon, pRK404(E) derivative, Tc^R	this study
pRKHTMHBgl	~5.1 kb *Eco*RI−*Pst*I fragment carrying *puf* operon with polyhistidine-tagged RC-M gene, pRK404(EH) derivative, Tc^R	this study
pRKHTL212-213AA	L212Glu-L213Asp→Ala-Ala, derivative of pRKHTMHBgl, Tc^R	this study
strains		
E. coli		
S17-1	*recA pro hsdR* RP4-2-Tc::Mu-Km::Tn7	(*29*)
R. sphaeroides		
PUC705-BA	*pucBA* (Km^R), derivative of wild-type 2.4.1	(*44*)
ΔΔ11	*pucBA* (Km^R) *pufQBALMX*(Sp^R), derivative of PUC705-BA	this study

for the transfer of the first proton to Q_B. In the AA RCs, Q_B becomes singly reduced, but the photocycle cannot continue beyond this point (*18*, *19*). In the absence of nearby acidic side chains at L212 and L213, the Q_B^- state is extremely stable in the AA mutant RC; its lifetime is ~12 s, as compared to 1.2 s for the WT RC [pH 8.0; (*19*)]. Since the photocycle cannot be completed, the AA strain is incapable of growth under photosynthetic conditions. Applying selective pressure for recovery of the photosynthetic phenotype, we subsequently isolated photocompetent phenotypic revertants from this strain. In RCs of some of the phenotypic revertants, a second-site compensatory mutation introduced a negatively charged residue or removed a positively charged residue. This type of compensatory mutation restores proton-transfer function even though those RCs still carry the engineered AA mutations (*17*−*22*). Since these phenotypic revertants still lack the proton-donating acidic residues at L212-L213 nearby Q_B, we are most interested in understanding the structural basis for the restoration of proton-transfer function that is induced by the often-distant compensatory mutations. At the present time, no conditions for crystallization of the *R. capsulatus* RC have been identified. However, structural information can be derived by constructing the equivalent mutations in the homologous RC of *R. sphaeroides*, which is amenable to structure determination by X-ray crystallography.

Until recently, the functional changes caused by any introduced mutations were interpreted based on the structure of the native RC. The assumption made by necessity was that any structural changes in a mutant RC would be confined to the chemical differences between the side chains of the mutant and native residues, which could be modeled by computer graphics based on general protein structural principles. These assumptions are presumed to be reasonable if the change is only a difference in charge (e.g., glutamic acid to glutamine) or a larger amino acid is changed to a smaller one (e.g., glutamic acid to alanine). But our recent results vide infra have shown that this is not the case. Based on X-ray diffraction studies of the AA mutant RC, we report here that mutation of L212Glu and L213Asp to alanines has unexpected structural consequences. In addition to the removal of potentially charged residues, the substitution of the smaller alanines influenced the orientations of neighboring residues, the positions of bound water molecules, and the position of Q_B. Their substitution also leads to a coordinated movement in the protein backbone—not only at and near the mutation site, but also in contiguous chain segments.

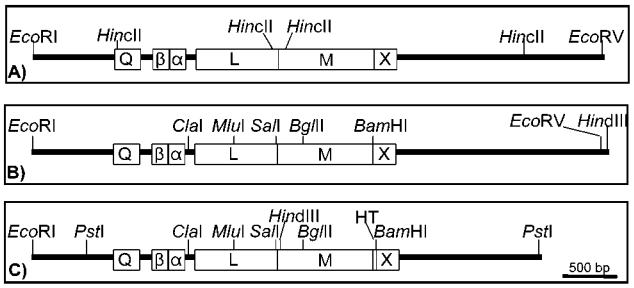

FIGURE 1: Restriction maps of cloned fragments of *R. sphaeroides* chromosomal DNA used in construction of the chromosomal deletion of the *puf* operon and its trans complementation (see also Table 1). Restriction sites relevant to the manipulations described in the text are shown. (A) *Eco*RI−*Eco*RV fragment of chromosomal DNA carrying *pufQBALMX* genes. To construct the deletion strain (see text), the three *Hin*cII fragments encompassing the operon were excised and replaced by a *Sma*I segment of pHP45Ω (*28*) encoding spectinomycin resistance. (B) Insert of complementing plasmid pRKMluBgl, carrying wild-type *Mlu*I-tagged L and *Bgl*II-tagged M genes. (C) Insert of complementing plasmid pRKHTMHBgl carrying a polyhistidine-tagged M gene (HT).

MATERIALS AND METHODS

(A) Expression System for R. sphaeroides RCs. Strains and plasmids described herein are listed in Table 1. Site-specific mutants of the *R. sphaeroides* RC were constructed via standard protocols (*26*) using an expression system that we have designed. This system consists of a deletion strain and a complementing plasmid. We used site-directed insertional mutagenesis to delete via homologous recombination a 4.1 kb segment that encompasses a portion of the *puf* operon in *R. sphaeroides* strain PUC705-BA (Table 1).

(i) Deletion Strain. To construct the deletion of the *puf* operon, an *Eco*RI−*Eco*RV fragment (Figure 1A) of plasmid pJW1 (*27*) carrying the *pufQBALMX* genes (and flanking

sequences) was subcloned into pIBI25 (International Biotechnologies, Inc.); this plasmid was designated pRIRV. Following complete digestion of pRIRV with *Hin*cII (Figure 1A), this plasmid was ligated to a *Sma*I fragment carrying a gene encoding streptomycin/spectinomycin resistance (Sp^R) derived from pHP45Ω (*28*). This interrupted *puf* operon was excised by double digestion with *Eco*RI and *Eco*RV. *Eco*RI linkers were ligated to the blunt *Eco*RV end before the fragment was subcloned into the *Eco*RI site of pSUP202 [$Ap^RCm^RTc^R$; (*29*)], a mobilizable plasmid that cannot be replicated in *R. sphaeroides*. This construct was designated pS202 ($Ap^RSp^RTc^R$). Following transfer of pS202 to the *R. sphaeroides* recipient strain PUC705-BA via conjugation with *E. coli* donor strain S17-1 (*29*), Sp^RTet^S exconjugants that had lost the *puf* operon as a result of a double-crossover event were selected. Replacement of the *puf* operon sequences with the Sp^R cassette was confirmed by hybridization of representative probes to digested chromosomal DNA. Deletion strain ΔΔ11 is $LHI^-LHII^-RC^-$; it is incapable of photosynthetic growth.

(ii) Complementing Plasmids. Two versions of a plasmid carrying *puf* operon genes were constructed to provide trans complementation of the chromosomal deletion. For the first plasmid, the above *Eco*RI−*Eco*RV fragment (Figure 1A) of pRIRV containing the wild-type *puf* operon was first subcloned into pBluescript SK (Ap^R; Stratagene); then the *Eco*RI site and a polylinker-encoded *Hin*dIII site flanking the *Eco*RV site were used to subclone the fragment into a derivative of broad-host-range vector pRK404 [pRK404(E), Tc^R; (*30*)]. Transfer of this complementing plasmid to ΔΔ11 via conjugation with S17-1 yields photocompetent, Tc^R "wild-type" transconjugants that are $LHI^+LHII^-RC^+$. For ease in shuttling mutant genes into this complementing plasmid, site-directed mutagenesis was used subsequently to engineer restriction sites to both flank and tag the L and M genes. A *Cla*I site was generated at an intergenic position that is 82 bp upstream of the L gene, and a *Bam*HI site was constructed at an intergenic position 4−6 bp downsteam of the termination codon for the M gene. A naturally occurring *Sal*I site is located at L261; thus, the majority of the L gene is borne on a *Cla*I−*Sal*I fragment, and the M gene is contained within a *Sal*I−*Bam*HI fragment. These fragments were subcloned separately into pBluescript II KS (Stratagene) for use as mutagenesis templates. Tagged versions of the L and M genes were created by introducing silent mutations within codons L145-L146 to create a unique *Mlu*I site, and within codons M88-M89 to create a unique *Bgl*II site. The resulting complementing plasmid was designated pRKMluBgl (inset shown in Figure 1B).

Recently, we developed a second version of the complementing plasmid in which a 7-histidine tail was appended to the 3′-end of the M gene. This C-terminal extension facilitates rapid and efficient recovery of purified RCs using immobilized metal affinity chromatography [IMAC; (*31*)]. A plasmid bearing the his-tagged M gene was obtained from S. Boxer [pRKSCH/pHisRC; (*9, 31, 32*)]. While incorporating the poly-histidine tag, features of pRKSCH/pHisRC and the above plasmid pRKMluBgl were merged in a series of manipulations (to be detailed elsewhere; P. D. Laible and D. K. Hanson, unpublished observations) in order to enhance the utility of this version of the complementing plasmid. These features included the incorporation of a silent *Hin*dIII site at codon L270 from pRKSCH/pHisRC and repair of the single *Hin*dIII site of pRK404(E) such that the site in the *puf* operon was unique [pRK404(EH); Table 1]. The engineered complementing segment contains unique *Cla*I, *Mlu*I, *Hin*dIII, *Bgl*II, and *Bam*HI sites that are useful for cloning or tagging genes as they are moved into or out of the expression plasmid. This segment was excised as a 5.1 kb fragment following partial digestion with *Eco*RI−*Pst*I. It was subcloned into pRK404(EH) and was designated pRKHTMHBgl (inset shown in Figure 1C).

Thus, complementing plasmids are available for the expression of native or his-tagged RCs, the choice depending on the experiments planned for purified RCs derived from the expression system.

(B) Mutant Construction. Oligonucleotides encoding the site-specific L212Glu-L213Asp→Ala-Ala mutations were designed to introduce a *Psp*1406I site in the L213 codon, and the mutant L gene was constructed according to directions from a kit (Chameleon; Stratagene). The presence of the desired mutations in candidates containing an additional *Psp*1406I site was confirmed by dideoxy sequencing (Sequenase 2.0 kit; United States Biochemical). The mutant L gene was then subcloned into pRKHTMHBgl; the resulting construct was designated pRKHTL212−213AA. This plasmid was then transferred to the *R. sphaeroides* deletion strain ΔΔ11 via conjugation with S17-1 (*29*).

(C) Growth of Mutant Strains. R. sphaeroides strains carrying mutant or wild-type expression plasmids were grown under chemoheterotrophic conditions (semi-aerobic, dark, 33 °C, 2 L of media in a 2.8 L Fernbach flask, 125 rpm) on YCC medium (*33*) containing tetracycline (1 μg/mL), in the absence of selection for RC function.

(D) Protein Preparation and Crystallization. The poly-histidine tail is on the periplasmic surface of the pigment−protein complex and associates readily with Ni−NTA (nitrilotriacetic acid) resin for rapid purification by IMAC. Starting from a cell suspension, extremely pure RCs were isolated using a 4−5 h protocol. The purification protocol was adapted from that of Goldsmith and Boxer (*31*) with modifications that have been described elsewhere (*34*). Pure proteins (those with an A_{280}:A_{800} ratio of ≤1.4) were taken directly from the IMAC column and were subsequently washed multiple times (in a Tris-HCl solution, pH 7.8, containing 0.09% LDAO) using a centrifugal concentrator [2000*g*; 50 kDa cutoff membrane (Millipore)] to remove imidazole from the buffer by successive dilution. When sufficiently imidazole-free, the RCs were concentrated to an A_{800} of 60−80 (1 cm path; 20−28 mg/mL) and were crystallized by a method similar to that described previously (*35*). In summary, equal parts of concentrated RC solution and a phosphate buffer (1.6 M potassium phosphate, pH 7.5, 4.2% dioxane, 7.35% heptanetriol, high-melting point isomer) were combined and constituted the initial crystallization conditions in sitting vapor diffusion droplets (typically 25 μL total volume). This RC mixture was equilibrated (at 25 °C) against a 1 mL reservoir of 1.6 M phosphate, pH 7.5. A small number of diffraction quality crystals commonly formed in the 1.6 M trials in 5−7 days; growth of crystals that were large enough for multiple translations during data collections required several weeks of incubation. Crystals were stabilized by equilibration with 2.0 M potassium phosphate, pH 7.5, in the reservoir for a minimum of 3 days.

Table 2: Crystallographic Data for WT and AA Mutant RCs[a]

	WT	AA
space group	$P3_121$	$P3_121$
unit cell dimensions		
$a = b$, Å	141.5	141.5
c, Å	187.2	187.4
highest resolution (last shell), Å	3.1 (3.21−3.10)	3.1 (3.21−3.10)
R_{merge} (last shell), %	9.6 (28.1)	9.9 (24.6)
average $I/\sigma(I)$ (last shell)	10.1 (3.5)	12.5 (3.6)
completeness (last shell), %	92 (87)	92 (85)
redundancy (last shell)	2.8 (2.7)	2.3 (2.1)
no. of reflections used 10.0−3.1 Å ($\geq 2\sigma\|F_o\|$)	31406	31830
R-factor (before rigid-body fitting)	0.204[b]	0.223[c]
R-factor (rigid-body refined)	0.199	0.216
R-factor (after rebuilding)	0.193	0.203
R-factor (after overall *B*-factor refinement)	0.180	0.189

[a] These mutant crystals are isomorphous to crystals of 1pcr and 1qov (Protein DataBank) that have the spacegroup $P3_121$ and unit cell dimensions of 1pcr: $a = b = 141.4$ Å, $c = 187.2$ Å; 1qov: $a = b = 142$ Å, $c = 186.8$ Å. [b] 1pcr used as search structure. [c] "In-house" wild-type structure used as search structure.

(E) Data Collection. We have not been successful in determining freezing conditions for our RC crystals; this issue has been problematic for several groups. Of the ten RC structures that have been determined from trigonal crystals that are obtained from high concentrations of phosphate, eight of which are deposited in the PDB, only one [1E14, 2.7 Å resolution; (*36*)] resulted from data collected from a frozen crystal. Even with freezing, two crystals were used by these investigators for data collection. According to K. McAuley (private communication, 1999), the resolution of the crystals observed at room temperature (2.1 Å) decreased to 2.6 Å resolution at best upon freezing. We have tried, unsuccessfully, to reproduce the tetragonal crystals described by Stowell et al. (*6*) that can be frozen.

We collected X-ray diffraction data at room temperature on an R-Axis IIc detector with X-rays generated using a rotating anode. Each crystal was mounted in a glass capillary with its long axis approximately parallel to the capillary (spindle) axis. Crystals diffracted to about 2.7 Å. Depending on its length, each crystal was exposed in two or three parts. Each segment was exposed for about 10 frames (with an oscillation angle of 0.7 or 0.8 Å and 30 min exposure per frame) and then translated along the long axis. Data were integrated with DENZO (*37*) and then merged and scaled with SCALEPACK (*37*). To minimize the effect of radiation damage, only frames with scale factors above 0.8 (indicating decay of <20%) were included in the final merged data. Data sets for both the wild-type and AA mutant RCs were collected with three crystals.

The cell parameters, data collection, and final model statistics are given in Table 2. Data sets were complete to 3.1 Å resolution. All subsequent calculations utilized 10.0−3.1 Å data. Rigid-body refinement and calculations of OMIT maps and electron density maps were done using the program CNS (*38*). The program CHAIN (*39*) was used for display and manual adjustments of the model. Approximately 11% of the atoms were moved in constructing the "in-house" WT structure from the search structures, and approximately 6% of the atom positions of the WT structure were altered to build the final AA structure. The rebuilt residues were regularized with the program CHAIN to optimize the geometry, but no crystallographic refinement of the resulting models was carried out, except for refinement of the overall isotropic *B*-factor. Individual isotropic *B*-factors were taken from 1pcr.

The structures of the WT and AA mutant RCs show that these relatively low-resolution diffraction data and the use of difference Fourier techniques are sensitive enough to see and identify the changes in positions of the main chain, side chains, and water molecules in the mutant RCs. Water molecules were considered observed if they had electron density in both the $3F_o - 2F_c$ and $F_o - F_c$ maps contoured at 1σ and 2.5σ, respectively, and had at least one hydrogen bond with another water molecule or with a protein atom. The positions of water molecules observed in the various RC structures were compared by determining the distance between them after the protein chains were overlapped. A water molecule in one RC structure was considered to be the equivalent of a water molecule in another RC structure if the distance between them was ≤1 Å. The contact distances were calculated with the program CHAIN (*39*).

The WT and AA mutant structures were compared by positioning the WT structure in the unit cell of the AA mutant RC by rigid-body refinement using the program CNS (*38*).

RESULTS

Data Quality. Diffraction data were of good quality, as shown by the information summarized in Table 2. Data sets were complete to 3.1 Å resolution on crystals that diffracted to 2.7 Å resolution. The diffraction of these crystals decreases such that by the last shell (3.1 Å) the intensities of the reflections are an order of magnitude weaker than the intensities observed in the first shell. At 2.7 Å, the intensities have decreased over 20-fold as compared to those observed in the first shell. By using only the 3.1 Å resolution data, we are able to use a large fraction of the significant reflections in our calculations to obtain excellent electron density maps.

Structure of the Wild-Type RC. Initially, the structure of the AA mutant RC was determined using the coordinates from the wild-type *R. sphaeroides* RC structure of Ermler et al. [PDB code: 1pcr; (*4*)] as the search structure. The coordinates for the structure of a mutant *R. sphaeroides* RC [A(M260)W mutation near Q_A; PDB code: 1qov (*40*)] were used as an ancillary guide during rebuilding. Electron density in some parts of the complex agreed well with the coordinates of 1pcr and in other parts agreed well with the coordinates of 1qov. In addition to structural changes introduced by the mutations, the electron density also suggested changes in distant parts of the complex that were not expected to be due to the amino acid substitutions. Therefore, it was impossible to determine what changes were mutation-related, so we decided to determine an "in-house" wild-type RC structure and compare the AA mutant RC structure to it.

The unit cell parameters ($a = b = 141.5$ Å, $c = 187.2$ Å) of our wild-type RC crystal were found to be essentially identical to that of 1pcr (unit cell dimensions $a = b = 141.4$ Å, $c = 187.2$ Å). Both crystals have the same space group, $P3_121$. Therefore, the 1pcr coordinates were used as the search structure in rigid-body refinement of the whole complex with our diffraction data. Detergent molecules, Q_B,

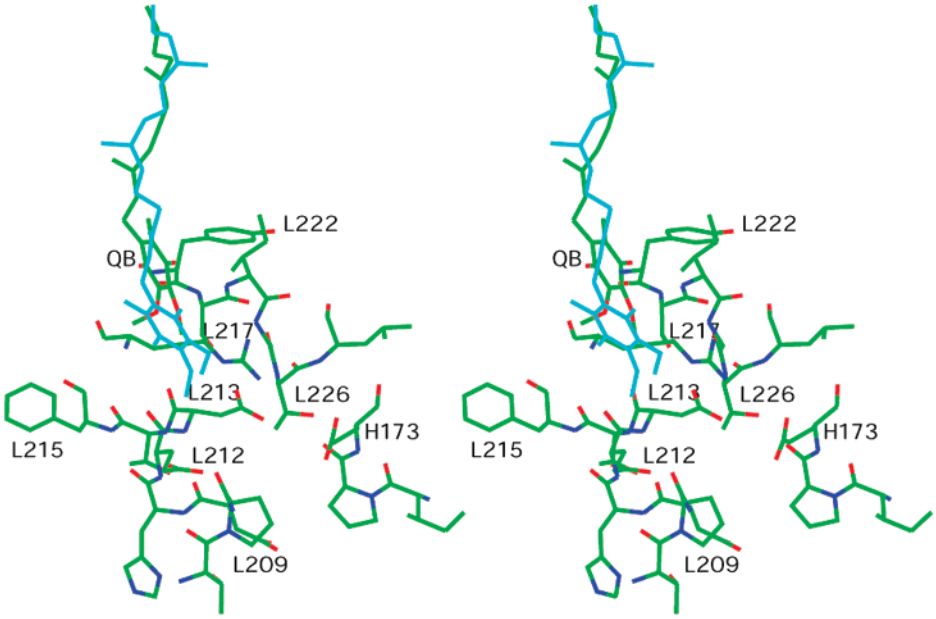

FIGURE 2: Stereoview showing the position of the secondary quinone, Q_B, relative to amino acid side chains in its immediate vicinity in the wild-type RC structure. The position of Q_B in the AA mutant RC structure is overlapped and shown in cyan.

and water molecules were removed from the search structure. The electron density maps (OMIT, $3F_o - 2F_c$, and $F_o - F_c$) calculated from the resulting model were of exceptional quality. Density was present for Q_B, water, and detergent molecules not included in the search structure. No residues beyond M302 can been seen, including the poly-histidine tag. The quality of the electron density map was indicated by the presence of clear density for a cardiolipin molecule located in the same position as reported by McAuley et al. in the structure of the A(M260)W mutant RC [1qov; unit cell dimensions $a = b = 142$ Å, $c = 186.8$ Å; (*41*)]. The 1qov RC structure was based on 2.1 Å resolution data, and it also crystallized in the same space group as 1pcr (resolution 2.65 Å). The cardiolipin molecule was not identified in 1pcr by Ermler et al. (*4*).

The 1pcr structure was rebuilt to fit our electron density maps; when possible, side chains were refitted to be in their most favored rotamer orientations. A total of 24 side chains—18 leucine residues, and arginine, valine, and isoleucine residues (2 each)—were in nonstandard conformations in the 1pcr model. In addition, several peptide bonds and aromatic rings (Phe, Tyr, and His) were found to be nonplanar in 1pcr. The structural model of the A(M260)W mutant RC (1qov) was found to fit the electron density better in several parts of the RC molecule, and therefore it was used as a guide in rebuilding our WT model at several locations in the protein chains as well as the substituents on the porphyrin rings. Orientations of the peptide bonds were rebuilt according to the 1qov structure between residues L31-L32, L201-L202, M52-M53, and H81-H82. The carotenoid geometry with the cis bond at 15,15′ of spheroidenone observed in the 1qov structure was a better fit to our electron density than the 13,-14 cis bond in spheroidene in 1pcr. Q_B was located in the site that is distal to the iron−ligand complex (Figure 2), as seen in the "dark" structure of Stowell et al. (*6*). The tail of Q_B is visible to carbon atom C19, and the orientation of the tail correlates with the orientation of the headgroup. Because of a lateral displacement, the headgroup is ~1 Å closer to residue L223Ser than is observed in the "dark" structure. In the 1pcr structure, Q_B is also bound in the distal site and has a high temperature factor; similarly, the electron density for the quinone was relatively weak in our WT structure as well, also indicating that the site is incompletely occupied. The side chain atoms of H173Glu are disordered based on electron density in our WT structure and on their high *B*-factors in 1pcr. H173Glu is also disordered in the "light" structure of Stowell et al. (*6*).

The rebuilt residues were regularized with the program CHAIN to optimize the geometry, but no crystallographic refinement of the resulting model was carried out. Coordinates of the entire complex—not just those of the affected sites—would have been adjusted to fit the crystallographic observations if refinement had been carried out. Refinement with relatively low-resolution data would have lead to a deterioration in the quality of the model of the complex.

The above rebuilding strategy led to the "in-house" version of the wild-type reaction center structure that was used to analyze the changes caused by the alanine substitutions in the structure of the AA mutant RC. The *R*-factors before and after rebuilding are 0.199 and 0.193, respectively, and 0.180 after overall isotropic *B*-factor refinement. The "in-house" wild-type RC structure has features common to both 1pcr and 1qov, and it also incorporates some additional changes that were made based on the OMIT, $3F_o - 2F_c$, and $F_o - F_c$ electron density maps. The minimal and maximal coordinate errors are 0.11 and 0.26 Å, respectively, as determined by SFCHECK (*42*). The structure was deposited in the Protein DataBank (PDB code: 1k6l).

Structure of the AA Mutant Reaction Center. In the AA mutant RC, residues L212Glu and L213Asp were changed to alanines. The AA mutant RC crystallized in the same space group as the WT, with unit cell dimensions $a = b = 141.5$ Å, $c = 187.4$ Å. The agreement between the data sets for the WT and AA crystals is good; the merging *R*-factor between the two data sets is 9.4% for all the data and 20% for the last shell. The coordinates of the "in-house" wild-

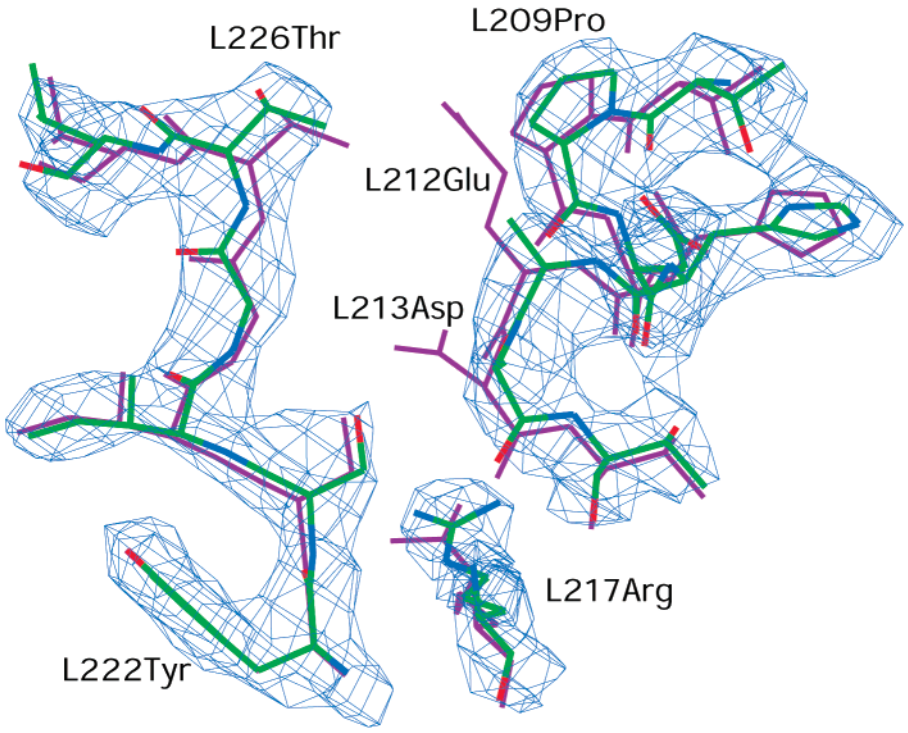

FIGURE 3: Electron density (calculated with coefficients $3F_o - 2F_c$, contoured at 1.5 σ) is shown for residues L208−L214 and L222−L227 and the side chain of residue L217Arg of the AA mutant RC. To illustrate the changes in orientations of both the main chain and side chains that are caused by the AA mutations, the structure of the wild-type RC with the native L212Glu and L213Asp residues is shown in purple. The two structures were overlapped as described in the text.

type RC structure were used for rigid-body refinement after removing atoms beyond Cβ for residues L212 and L213; Q_B, water, and detergent molecules were also excluded. The resulting model was used to calculate an OMIT map, and $3F_o - 2F_c$ and $F_o - F_c$ electron density maps. In addition, a map with $F_{o(AA)} - kF_{o(WT)}$ coefficients using phases from the wild-type structure was examined. The electron density indicated that alanines are now present at positions L212 and L213 (Figure 3). Previous changes made in the WT RC structure compared to 1pcr also fit the electron density calculated with the AA diffraction data. Although the changes introduced by the AA mutations were numerous and coordinated (vide infra), it was very gratifying to see that the differences with the "in-house" wild-type RC structure were mostly localized to the contiguous chain segments affected by the L212-L213 mutations. Differences observed included the movement of Q_B into the proximal binding site near the iron−ligand complex—3.5 Å from the distal position that it occupies in the structure of the WT protein (Figure 2). In the AA structure, Q_B is 0.8 Å more distal than was seen in the "light" structure of Stowell et al. (*6*). Q_B has more density in the AA structure than it does in the WT structure, but the site is probably not fully occupied. Most of the density is in the proximal position. Electron density for the tail of Q_B is visible until carbon atom C24.

There were very minor changes between the "in-house" wild-type RC structure and other parts of the AA RC structure outside of the region directly affected by the mutations. This similarity might be expected because the systematic errors between the two structures were minimized since the crystals were grown under the same conditions and the data were collected and processed in the same way. The electron density clearly showed where changes were required due to the mutations. The above-mentioned maps were used to rebuild the parts of the molecule that were affected by the mutations. The *R*-factors before and after rebuilding are 0.216 and 0.203, respectively. The *R*-factor after overall isotropic *B*-factor refinement is 0.189. The minimal and maximal coordinate error is 0.10 and 0.28 Å, respectively, as determined by SFCHECK (*42*). The structure was deposited in the Protein DataBank (PDB code: 1k6n).

Water Molecules. Water molecules are important components of the interactive network that delivers protons to the quinone anions. Crystallographic techniques can identify water molecules if they occupy a fixed position in the structure most of the time. In general, water molecules are not fixed; therefore, they have high temperature factors and contribute only to the relatively low-resolution reflections. Electron densities can be identified as water molecules with high confidence if the phases (based on the rest of the structure) are accurate. Highly accurate structures are usually obtained with high-resolution data, but once the structure is known it can be used for phasing data where the resolution is not as high.

Using the strict criteria defined under Materials and Methods, we identified 138 water molecules in our "in-house" wild-type RC structure and 129 water molecules in the structure of the AA mutant RC (Table 3). Of fifteen water molecules that were observed in the WT structure but not in the AA structure, only one was in the mutation site. The remainder were surface-accessible water molecules and had very weak or no density in the AA structure. Of six water molecules observed in the AA structure only, one is near L213 and another is near H173 (discussed below). The rest were surface waters with very weak or no density in the WT structure. Of the 138 water molecules in our WT structure, 103 were previously seen in the 1pcr WT structure. Our WT structure also shares 103 water molecules with the 1qov

Table 3: Comparison of Water Molecules Observed in RC Structures

structure	WT	AA	1pcr (WT)	1qov [A(M260)W]
no. of waters observed	138[a]	129	160	250[b]
no. of waters in common with WT (≤1.0 Å distant)	−	121	103[c]	103[d]

[a] Eighteen of these waters had no equivalent in either 1pcr or 1qov. [b] Only 104 of these waters are within 1.0 Å from a water observed in 1pcr. [c] Eighteen of these waters are not in 1qov. [d] Sixteen of these waters are not in 1pcr.

structure [A(M260)W mutant]. However, different sets of water molecules were found in common with the 1pcr and 1qov structures. Although 160 and 250 water molecules were observed in the 1pcr and 1qov structures, respectively, only 104 of them were common to both structures. Eighteen water molecules that were identified in our WT structure have not been previously seen in either 1pcr or 1qov.

DISCUSSION

We have determined the structure of a modified RC: the L212Glu-L213Asp→Ala-Ala double mutant (AA) that blocks proton delivery to the secondary quinone Q_B. In addition, we have determined an "in-house" structure of the wild-type RC (WT). The incorporation of the poly-histidine affinity tag and the use of IMAC enabled us to obtain exceptionally pure mutant protein that formed diffraction-quality crystals. Data collected on these crystals resulted in excellent electron density maps that clearly showed the effects of the mutations. The rms deviation between all of the α-carbon positions of the WT and AA mutant structures is 0.07 Å.

Mutations Cause Many Coordinated Movements. As a result of L212Glu→Ala and L213Asp→Ala mutations, the chain segment L207−L227 moved; the displacement was largest for residues L207−L213 (0.5 Å) and L223−L227 (0.3−0.7 Å). These residues form the stems of the loop that sequesters the Q_B molecule. The location of the above segment (from the WT structure) relative to the position of Q_B in the WT and AA structures is shown in Figure 2. The loop became wider in the AA mutant (Figure 3). The distance between α carbons of L209Pro and L226Thr increased by about 1 Å from 7.4 Å in the WT structure to 8.5 Å in the AA mutant RC structure. A ripple effect of this change manifested itself in the displacement of neighboring chain segments H67−H68 (0.2−0.3 Å), H123−H126 (0.1 Å), and M21−M23 (0.1−0.7 Å) that are close to residues of the L207−L211 segment. Near residue L226, chain segment H172−H174 moved (0.2−0.4 Å), which in turn affected the positions of M44Asn (0.2 Å) and chain segment M11−M13 (0.2−0.4 Å). The movement of chain segment M11−M13 influenced the position of H141His (0.2 Å). The position of side chain L193Leu in the Q_B cavity also changed. Residue L193 is close to L212Glu in the WT structure. Interestingly, the positions of L216Phe and L222Tyr did not change. L216Phe is close to Q_B, and L222Tyr forms a hydrogen bond with the carbonyl oxygen of M44Asn. This hydrogen bond contributes to the integrity of the complex by holding together two chain segments from different subunits.

The correlated changes between chain segments in the structure of the AA RC allow for the maintenance of all of the hydrogen bonds and salt bridges between them. The hydrogen bonds are maintained between the carbonyl oxygen of M13Arg and the peptide nitrogen of H141His (2.9 Å), between the peptide nitrogen of M14Gly and OE1 of H174Gln (3.0 Å), and between the peptide nitrogen of H125Gly and OD2 of L210Asp (2.8 Å). A small change occurred in the length of the hydrogen bond between the carbonyl oxygen of H124Asp and NE2 of H68His (the distances are 2.6 and 2.8 Å, respectively, for the AA and WT RC structures). The carboxyl oxygen OE1 of H173Glu forms a hydrogen bond (3.2 Å) with the peptide nitrogen of L226Thr in the AA structure, while in the WT structure the same oxygen forms a hydrogen bond (2.9 Å) with the side chain OG1 atom of L226Thr. The carboxyl oxygen OE1 of M22Glu forms a salt bridge (4.0 Å) in both structures with NH1 of L207Arg.

Residues L212Glu and L213Asp are part of an interactive network of charged residues at the interface of the L, M, and H chains located on the cytoplasmic side of the Q_B cofactor. Upon mutating these two acidic residues to neutral alanines, some of the distances between the residues of the network changed. The removal of two potentially negatively charged residues upsets the balance of charged residues near the Q_B site and leads to their rearrangement, which we observe. The closest charged residues to L212Glu and L213Asp in the WT structure are L217Arg and H173Glu. In the structure of the AA mutant RC, residue L217Arg becomes closer to M17Asp, M44Asn, and H173Glu (4.5 vs 5.2 Å, 3.3 vs 3.6 Å, and 7.9 vs 8.9 Å). H173Glu moves closer to H177Arg, but further from H130Lys (3.4 vs 3.8 Å and 4.3 vs 3.3 Å). The realignment of charged residues might be the driving force that leads to movements not only of side chains but also of main chain atoms of the AA mutant RC as compared to the WT. We suggest that this rearrangement is responsible for the unexpected finding that the chain segment that contains L212 and L213 moves further from its neighboring L223−L226 chain segment instead of closer to it, as would be expected upon substituting smaller alanines for larger acidic residues. We had predicted that such "electrostatic domino" movements would be the consequences of disruption of a portion of a large interacting web of ionizable residues and water molecules (*22*). Realignments of residue−residue, water−water, and residue−water interactions would be necessary after substitution of an interactive partner by a nonpolar residue.

Residues showing major differences in side chain geometry in addition to the movement of the main chain segments are L207Arg, L217Arg, M21Thr, M22Glu, M86Leu, M292Asp, H118Arg, H128His, and H173Glu. In contrast to the wild-type structure where the electron density is discontinuous (Figure 4A), the electron density for the side chain of H173Glu can be seen clearly in the electron density map of the AA mutant RC (Figure 4B). [In the wild-type RCs of Stowell et al. (*6*), H173Glu is ordered in the "dark" structure and is disordered in the "light" structure.] H173Glu is part of the cluster of negatively charged residues that delivers protons to the secondary quinone (*14*) and was recently proposed to be involved in the gating process of the first electron transfer (*24*). In the structure of the AA RC, H173Glu has an altered conformation—its position changed by a maximum of 1.3 Å. In the structure of the wild-type RC, H173Glu forms a salt bridge with H130Lys, whereas in the AA structure an extra water molecule is found between

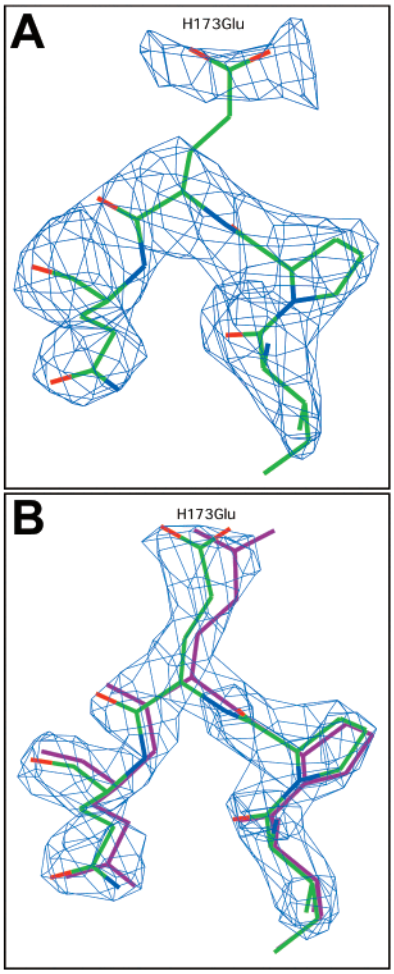

FIGURE 4: (A) Electron density (calculated with coefficients $3F_o - 2F_c$, contoured at 1.5 σ) is shown for residues H171−H174 of the wild-type RC. The electron density for the side chain of H173Glu is discontinuous, indicating that it is disordered. (B) Electron density (calculated with coefficients $3F_o - 2F_c$, contoured at 1.5 σ) is shown for residues H171−H174 of the AA mutant RC. Unlike the situation for the WT RC, there is clear density for H173 in the structure of this mutant RC. To illustrate the change in the structure caused by the AA mutations, the structure of the wild-type RC (purple) is also shown. The two structures were overlapped as described in the text.

H130Lys and H173Glu and the hydrogen bond is formed through this water molecule (Figure 5). The water molecule is located where the OE2 atom of H173 was located in the structure of the wild-type RC. In the new position, H173Glu also forms a hydrogen bond with the backbone amide nitrogen of residue L226; this hydrogen bond is not observed in the wild-type RC structure. A water molecule that formed hydrogen bonds with H173Glu and L213Asp in the structure of our WT RC (not observed in the 1pcr WT RC) is no longer present. Instead, a water molecule is now found near L213Ala; it replaces the aspartic acid side chain observed at this position in the structure of the WT RC. This water is hydrogen-bonded to both L223Ser and M44Asn (see Figure 6).

Binding Site of Q_B. The position of Q_B in the structure of the AA RC differs from that found in the WT RC structure (Figure 2); it is in a proximal position more similar to the one observed in the structure of the A(M260)W mutant RC [1qov; (*41*)]. In previous studies, the position of Q_B was found to be dependent on the illumination state of the

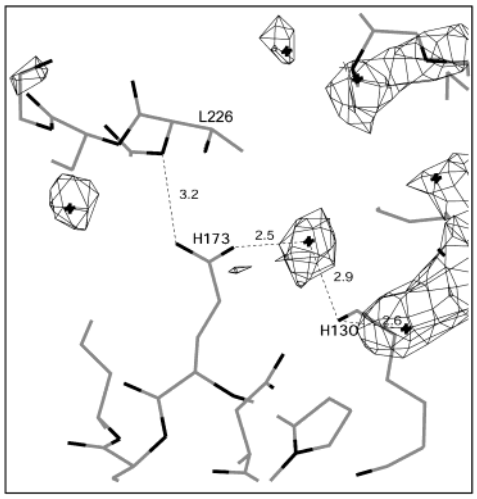

FIGURE 5: Residue H173Glu and the position of a water molecule that compensates for the movement of H173Glu in the structure of the L212Ala-L213Ala mutant RC. This "new" water molecule forms a bridge between H173Glu and H130Lys. In the wild-type RC structure, these residues are directly hydrogen-bonded to each other. (Difference electron density, contoured at 3 σ, shows several additional water molecules indicated by +. The water molecules were not included in the structure factor calculations.)

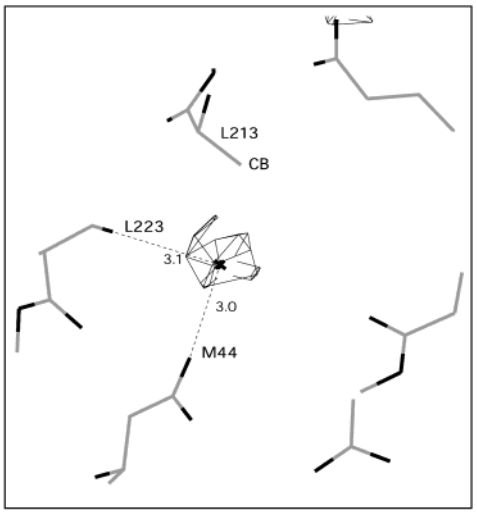

FIGURE 6: Difference electron density, contoured at 3 σ, showing the water molecule that replaces the L213Asp residue in the structure of the L212Glu-L213Asp→Ala-Ala double mutant RC. This water forms hydrogen bonds with L223Ser and M44Asn. (The water molecules were not included in the structure factor calculations.)

crystal—in a dark-adapted crystal, Q_B was bound in the distal position, while in the light-adapted crystal, Q_B was located in the proximal site (*6*). In our wild-type RC structure, Q_B is present in the distal position where it was observed in 1pcr and in the L181Phe→Lys mutant (P. R. Pokkuluri, A. N. Hata, T. N. Wong, P. D. Laible, D. K. Hanson, and M. Schiffer, unpublished observations). Although the data for the AA crystal were collected in the same way, Q_B was bound mostly in the proximal position in the structure of this RC, as seen in the structure of the A(M260)W mutant RC previously (*41*). Q_B was also observed to be in the proximal position in the structure of the L209Pro→Tyr mutant RC (*43*). An intermediate position for Q_B was observed in the structure of the L209Pro→Phe mutant RC (*43*). If our new data are taken together with the previously

published structures, the position of Q_B might be correlated with the mutation of residues near the quinone sites.

Conclusions. The structure of the RC from the photosynthetically incompetent AA mutant revealed unexpected changes from the structure of the wild-type RC of *R. sphaeroides*. Unexpectedly, in response to the replacement of these large ionizable side chains by smaller nonpolar side chains, we observed a concerted movement of chain segments of all three RC subunits that interact to form the Q_B binding site in the cytoplasmic region of the complex. Counterintuitively, the alanine substitutions caused an expansion of the cavity rather than its collapse. The primary density of Q_B in the structure of the AA RC shifted (3.5 Å) from a position relatively far from the iron−ligand complex to a position proximal to it. This movement of Q_B may be a reaction to the observed expansion of the binding pocket that accompanied the engineered amino acid substitutions. We are anxious to determine which, if any, of these structural changes are reversed or modified in RCs derived from photocompetent phenotypic revertant strains that carry distant compensatory mutations. Since both L212Glu and L213Asp are still missing in these revertant RCs, auxiliary proton delivery pathways rather than the native pathway must be operative. By integrating the results of spectroscopic experiments with structure determination experiments, we will be able to determine the structural requirements that lead to the activation of robust, alternative pathways for protein-mediated proton transfer.

REFERENCES

1. Deisenhofer, J., Epp, O., Miki, K., Huber, R., and Michel, H. (1985) Structure of the protein subunits in the photosynthetic reaction center from *Rhodopseudomonas viridis* at 3 Å resolution. *Nature 318*, 618−624.
2. Allen, J. P., Feher, G., Yeates, T. O., Komiya, H., and Rees, D. C. (1987) Structure of the reaction center from *Rhodobacter sphaeroides* R-26: The cofactors. *Proc. Natl. Acad. Sci. U.S.A. 84*, 5730−5734.
3. Chang, C.-H., El-Kabbani, O., Tiede, D. M., Norris, J. R., and Schiffer, M. (1991) The structure of the membrane-bound photosynthetic reaction center from *Rhodobacter sphaeroides*. *Biochemistry 30*, 5352−5360.
4. Ermler, U., Fritsch, G., Buchanan, S. K., and Michel, H. (1994) Structure of the photosynthetic reaction centre from *Rhodobacter sphaeroides* at 2.65 Å resolution: cofactor and protein−cofactor interactions. *Structure 2*, 925−936.
5. Arnoux, B., Gaucher, J. F., Ducruix, A., and Reiss, F. (1995) Structure of the photochemical reaction center of a spheroidene-containing purple bacterium, *Rhodobacter sphaeroides* Y, at 3 Å resolution. *Acta Crystallogr. D51*, 368−379.
6. Stowell, M. H. B., McPhillips, T. M., Rees, D. C., Soltis, S. M., Abresch, E., and Feher, G. (1997) Light-induced structural changes in photosynthetic reaction center: Implications for mechanism of electron−proton transfer. *Science 276*, 812−816.
7. McAuley-Hecht, K. E., Fyfe, P. K., Ridge, J. P., Prince, S. M., Hunter, C. N., Isaacs, N. W., Cogdell, R. J., and Jones, M. R. (1998) Structural studies of wild-type and mutant reaction centers from an antenna-deficient strain of *Rhodobacter sphaeroides*: Monitoring the optical properties of the complex from bacterial cell to crystal. *Biochemistry 37*, 4740−4750.
8. Lancaster, C., and Michel, H. (1997) The coupling of light-induced electron transfer and proton uptake as derived from crystal structures of reaction centres from *Rhodopseudomonas viridis* modified at the binding site of the secondary quinone, Q_B. *Structure 5*, 1339−1359.
9. Paddock, M. L., Rongey, S. H., Feher, G., and Okamura, M. Y. (1989) Pathway of proton transfer in bacterial reaction centers: Replacement of glutamic acid 212 in the L subunit by glutamine inhibits quinone (secondary acceptor) turnover. *Proc. Natl. Acad. Sci. U.S.A. 86*, 6602−6606.
10. Paddock, M. L., McPherson, P. H., Feher, G., and Okamura, M. Y. (1990) Pathway of proton transfer in bacterial reaction centers: Replacement of serine-L223 by alanine inhibits electron and proton transfers associated with reduction of quinone to dihydroquinone. *Proc. Natl. Acad. Sci. U.S.A. 87*, 6803−6807.
11. Paddock, M. L., Rongey, S. H., McPherson, P. H., Juth, A., Feher, G., and Okamura, M. Y. (1994) Pathway of proton transfer in bacterial reaction centers: Role of aspartate-L213 in proton transfers associated with reduction of quinone to dihydroquinone. *Biochemistry 33*, 734−745.
12. Takahashi, E., and Wraight, C. A. (1990) A crucial role for AspL213 in the proton-transfer pathway to the secondary quinone of reaction centers from *Rhodobacter sphaeroides. Biochim. Biophys. Acta 1020*, 107−111.
13. Takahashi, E., and Wraight, C. A. (1992) Proton and electron transfer in the acceptor quinone complex of *Rb. sphaeroides*: Characterization of site-directed mutants of the two ionizable residues, GluL212 and AspL213, in the Q_B binding site. *Biochemistry 31*, 855−866.
14. Takahashi, E., and Wraight, C. A. (1996) Potential of proton-transfer function by electrostatic interactions in photosynthetic reaction centers from *Rhodobacter sphaeroides*: First results from site-directed mutation of the H subunit. *Proc. Natl. Acad. Sci. U.S.A. 93*, 2640−2645.
15. Bylina, E. J., Jovine, R. V. M., and Youvan, D. C. (1989) A genetic system for rapidly assessing herbicides that compete for the quinone binding site of photosynthetic reaction centers. *Bio/Technology 7*, 69−74.
16. Bylina, E. J., and Wong, R. (1992) in *Research in Photosynthesis* (Murata, N., Ed.) pp 369−372, Kluwer Academic Publishers, Dordrecht, The Netherlands.
17. Hanson, D. K., Nance, S. L., and Schiffer, M. (1992) Second-site mutation at M43 (Asn → Asp) compensates for the loss of two acidic residues in the Q_B site of the reaction center. *Photosynth. Res. 32*, 147−153.
18. Schiffer, M., Chan, C.-K., Chang, C.-H., DiMagno, T. J., Fleming, G. R., Nance, S. L., Norris, J. R., Snyder, S., Thurnauer, M. C., Tiede, D. M., and Hanson, D. K. (1992) in *The Photosynthetic Bacterial Reaction Center II, NATO ASI Series* (Breton, J., and Vermeglio, A., Eds.) pp 251−261, Plenum Press, London.
19. Hanson, D. K., Baciou, L., Tiede, D. M., Nance, S. L., Schiffer, M., and Sebban, P. (1992) In bacterial reaction centers, protons can diffuse to the secondary quinone by alternative pathways. *Biochim. Biophys. Acta 1102*, 260−265.
20. Hanson, D. K., Tiede, D. M., Nance, S. L., Chang, C.-H., and Schiffer, M. (1993) Site-specific and compensatory mutations imply unexpected pathways for proton delivery to the Q_B binding site of the photosynthetic reaction center. *Proc. Natl. Acad. Sci. U.S.A. 90*, 8929−8933.
21. Maróti, P., Hanson, D. K., Baciou, L., Schiffer, M., and Sebban, P. (1994) Proton conduction within the reaction center of *Rhodobacter capsulatus*: the electrostatic role of the protein. *Proc. Natl. Acad. Sci. U.S.A. 91*, 5617−5621.
22. Sebban, P., Maróti, P., Schiffer, M., and Hanson, D. K. (1995) Electrostatic dominoes: Long distance propagation of mutational effects in photosynthetic reaction centers of *Rhodobacter capsulatus. Biochemistry 34*, 8390−8397.
23. Paddock, M. L., Graige, M. S., Feher, G., and Okamura, M. Y. (1999) Identification of the proton-transfer pathway in bacterial reaction centers: Inhibition of proton transfer by binding of Zn^{2+} or Cd^{2+}. *Proc. Natl. Acad. Sci. U.S.A. 96*, 6183−6188.
24. Paddock, M. L., Feher, G., and Okamura, M. Y. (2000) Identification of the proton pathway in bacterial reaction centers: Replacement of Asp-M17 and Asp-L210 with Asn reduces the proton-transfer rate in the presence of Cd^{2+}. *Proc. Natl. Acad. Sci. U.S.A. 97*, 1548−1553.

25. Axelrod, H. L., Abresch, E. C., Paddock, M. L., Okamura, M. Y., and Feher, G. (2000) Determination of the binding sites of the proton-transfer inhibitors Cd^{2+} and Zn^{2+} in bacterial reaction centers. *Proc. Natl. Acad. Sci. U.S.A. 97*, 1542−1547.
26. Sambrook, J., Fritsch, E., and Maniatis, T. (1989) *Molecular cloning: A laboratory manual*, 2nd ed., Cold Spring Harbor Press, Cold Spring Harbor, NY.
27. Williams, J. C., Steiner, L. A., Ogden, R. C., Simon, M. I., and Feher, G. (1983) Primary structure of the M subunit of the reaction center from *Rhodopseudomonas sphaeroides*. *Proc. Natl. Acad. Sci. U.S.A. 80*, 6505−6509.
28. Prentki, P., and Krisch, H. M. (1984) In vitro insertional mutagenesis with a selectable DNA fragment. *Gene*, 303−313.
29. Simon, R., Priefer, U., and Puhler, A. (1983) A broad host range mobilization system for in vivo genetic engineering: Transposon mutagenesis in gram negative bacteria. *Bio/Technology 1*, 37.
30. Ditta, G., Schmidhauser, T., Yakobsen, E., Lu, P., Liang, X.-W., Finlay, D. R., Guiney, D., and Helinski, D. R. (1985) Plasmids related to the broad host range vector, pRK290, useful for gene cloning and for monitoring gene expression. *Plasmid 13*, 149−153.
31. Goldsmith, J. O., and Boxer, S. G. (1996) Rapid isolation of bacterial photosynthetic reaction centers with an engineered poly-histidine tag. *Biochim. Biophys. Acta 1276*, 171−175.
32. Williams, J. C., Alden, R. G., Murchison, H. A., Peloquin, J. M., Woodbury, N. W., and Allen, J. P. (1992) Effects of mutations near the bacteriochlorophylls in reaction centers from *Rhodobacter sphaeroides*. *Biochemistry 31*, 11029−11037.
33. Taguchi, A. K. W., Stocker, J. W., Alden, R. G., Causgrove, T. P., Peloquin, J. M., Boxer, S. G., and Woodbury, N. W. (1992) Biochemical characterization and electron-transfer reactions of *sym1*, a *Rhodobacter capsulatus* symmetry mutant which affects the initial electron donor. *Biochemistry 31*, 10345−10355.
34. Kirmaier, C., Czarnecki, K., Laible, P. D., Hata, A. N., Hanson, D. K., Bocian, D. F., and Holten, D. (2002) Comparison of M-side electron transfer in *Rb. sphaeroides* and *Rb. capsulatus* reaction centers. *J. Phys. Chem. B 106*, 1799−1808.
35. Buchanan, S. K., Fritzsch, G., Ermler, U., and Michel, H. (1993) New crystal form of the photosynthetic reaction centre from *Rhodobacter sphaeroides* of improved diffraction quality. *J. Mol. Biol. 230*, 1311−1314.
36. Fyfe, P. K., Ridge, J. P., McAuley, K. E., Cogdell, R. J., Isaacs, N. W., and Jones, M. R. (2000) Structural consequences of the replacement of glycine M203 with aspartic acid in the reaction center from *Rhodobacter sphaeroides. Biochemistry 39*, 5953−5960.
37. Otwinowski, Z., and Minor, W. (1997) Processing of X-ray diffraction data collected in oscillation mode. *Methods Enzymol. 276*, 307−326.
38. Brunger, A. T., Adams, P. D., Clore, G. M., Delano, W. L., Gros, P., Grosse-Kunstleve, R. W., Jiang, J.-S., Kuszewski, J., Nigles, M., Pannu, N. S., Read, R. J., Rice, L. M., Simonson, T., and Warren, G. L. (1998) Crystallography and NMR system: a new software suite for macromolecular structure determination. *Acta Crystallogr. D54*, 905−921.
39. Sack, J. S. (1988) CHAIN−A crystallographic modeling program. *J. Mol. Graphics 6*, 224−225.
40. McAuley, K. E., Fyfe, P. K., Ridge, J. P., Cogdell, R. J., Isaacs, N. W., and Jones, M. R. (2000) Ubiquinone binding, ubiquinone exclusion, and detailed cofactor conformation in a mutant bacterial reaction center. *Biochemistry 39*, 15032−15043.
41. McAuley, K. E., Fyfe, P. K., Ridge, J. R., Isaacs, N. W., Cogdell, R. J., and Jones, M. R. (1999) Structural details of an interaction between cardiolipin and an integral membrane protein. *Proc. Natl. Acad. Sci. U.S.A. 96*, 14706−14711.
42. Vaguine, A. A., Richelle, J., and Wodak, S. J. (1999) SFCHECK: a unified set of procedures for evaluating the quality of macromolecular structure-factor data and their agreement with the atomic model. *Acta Crystallogr. D55*, 191−205.
43. Kuglstatter, A., Ermler, U., Michel, H., Baciou, L., and Fritzsch, G. (2001) X-ray structure analyses of photosynthetic reaction center variants from *Rhodobacter sphaeroides*: Structural changes induced by point mutations at position L209 modulate electron and proton transfer. *Biochemistry 40*, 4253−4260.
44. Lee, J. K., Kiley, P. J., and Kaplan, S. (1989) Posttranscriptional control of *puc* operon expression of B800−850 light-harvesting complex formation in *Rhodobacter sphaeroides. J. Bacteriol. 171*, 3391−3405.

BI0118963